https://doi.org/10.1016/j.scriptamat.2021.113826

A novel $L1_2$-strengthened multicomponent Co-rich high-entropy alloy with both high γ'-solvus temperature and superior high-temperature strength

B.X. Cao [a], H.J. Kong [b], Z.Y. Ding [c], S.W. Wu[a], J.H. Luan[a], Z.B. Jiao[c], J. Lu[a,d], C.T. Liu[a,b,e,*],T. Yang [a,e,*]

[a] *Department of Materials Science and Engineering, City University of Hong Kong, Hong Kong, China*

[b] *Department of Mechanical Engineering, City University of Hong Kong, Hong Kong, China*

[c] *Department of Mechanical Engineering, The Hong Kong Polytechnic University, Hong Kong, China*

[d] *Department of Mechanical Engineering, City University of Hong Kong, Greater Bay Joint Division, Shenyang National Laboratory for Materials Science, Tat Chee Avenue, Kowloon, Hong Kong, China*

[e] *Hong Kong Institute for Advanced Study, City University of Hong Kong, Hong Kong, China*

Abstract

A $L1_2$-strengthened multicomponent Co-rich high-entropy alloy with superior microstructural stability was developed in this study. High-density cuboidal γ' particles were found to embed in the matrix for the alloy subjected to isothermal aging at temperatures ranging from 800 to 1100℃ without the formation of brittle intermetallic phases neither at grain boundaries nor grain interior after long-term thermal exposure. Atom probe analyses indicated that Ta and Nb elements preferentially partitioned to the γ' intermetallic phase, which is found to be substantially important for stabilizing the $L1_2$ ordered crystalline structure. More importantly, the present alloy exhibited a good combination of both high γ'-solvus temperature (1125℃) and low mass density ($8.28 gcm^{-3}$), together with superb high-temperature tensile strength (755MPa at 800℃ and 664 MPa at 900°C). The present findings offer an essential paradigm for designing

advanced $L1_2$-strengthened high-temperature alloys with broader temperature capabilities based on Co.

Keywords: Co-rich high-entropy alloy Microstructural stability Solute partitioning High-temperature strength

The development of modern aerospace engineering and power generation industry puts forward an urgent request for structural materials with superior temperature capabilities[1–3]. Ni-based superalloys strengthened by ordered $L1_2$ (γ') intermetallic compounds have been widely employed to cope with extreme service conditions[4,5]. However, Ni-based superalloys are believed to have approached their temperature limit due to the narrow gap between the γ'-solvus temperature and the melting temperature[6]. Consequently, it motivates the search for new classes of structural materials with higher upper temperature limits. Co-based alloys demonstrate a higher temperature capability, which is inherent in the higher melting temperature of Co as compared with that of Ni. Recently, the discovery of ordered γ'-Co_3(Al, W) intermetallic phase in the ternary Co-Al-W alloy system demonstrated the possibility of utilizing ordered precipitation for strengthening among Co-based high-temperature structural materials[7].

Despite a high γ'-phase volume fraction at room temperature and attractive mechanical performance among the $L1_2$-strengthened Co-Al-W superalloys, several drawbacks still limit their wide engineering applications. Stabilization of the γ' phase at elevated temperatures is a critical issue in designing $L1_2$-strengthened Co-based

superalloys. It is noted that the γ'-solvus temperature continuously increased as the replacement of Co with Ni content in Co-10Al-10W (the unit of at.% is also used in the remainder of the article unless specified) alloy[8].Due to the large solubility of Ni in Co-based superalloys, it depicts a vast alloy design space between Co-based and Ni-based superalloys by utilizing Ni additions for the stabilization of the thermodynamically metastable γ' phase in Co-based alloys. It has also been demonstrated that certain transition metals contribute to the stability of the γ' phase[9,10]. For example, the additions of Ti and Ta significantly increased the γ'-solvus temperature to 1131℃ in a Co-Al-W-based superalloy[11]. On the other hand, excessive γ'-stabilization elements and complicated elemental interactions increased the propensity for detrimental intermetallic phase formation, if the alloy compositions are not well properly optimized[12]. Moreover, the high-energy grain boundary regions often act as preferential sites for heterogeneous precipitation of undesired intermetallic phases, which make grain boundaries more vulnerable during long-term isothermal heat treatments. For example, in the Co-6Ta-6V alloy metastable γ' phase was consumed by discontinuous C36-type Laves phase at 900℃, implying that the Laves phase is the equilibrium phase at 900℃[13]. Similarly, the formation of the $D0_{19}$-type and B2-type intermetallic phases at grain boundaries was also observed in the Co-10Ni-7Al-4Ti-5Mo-2Nb and Co-5.6Al-5.8W-6.6Ti-0.12B alloys[14,15]. Tetragonal close-packed μ phase with a composition of $(Co, Ni)_7(Ta, Mo)_6$ was detected along grain boundaries in a CoNi-based superalloy[16]. Deleterious intermetallic phases formation at grain boundaries are believed to cause severe property degradation by acting as sites for crack

initiation and propagation, and all of these significantly weaken the grain boundaries, leading to permanent intergranular fracture at an early stage of plastic deformation[17,18]. Besides, these intermetallic phases usually deplete refractory elements (Mo, W, Nb, Ta) from the γ matrix, thus weakening the effectiveness of solid-solution strengthening and accelerating γ' coarsening by influencing the solute diffusion in the γ matrix[14]. Consequently, the optimization of these γ'-stabilizing element concentrations is vital for the design of γ'-strengthened Co-based superalloys. This sets the research for the current design effort.

Mass density is another critical evaluation criterion in designing structural materials for aerospace engineering, whereas the incorporation of a large amount of W additions adversely affects it. Recently, the development of W-free Co-based superalloys with a reduced mass density has received a priority attention[19,20]. Replacing W with Mo led to the discovery of a series of Co-Al- Mo-based superalloys[9,21,22]. The mass density of the W-free Co-10Al-5Mo-2Nb alloy is 8.38 g cm^{-3}[21], which is comparable to commercial Ni-based superalloy (in the range of 7.9 - 8.5 g cm^{-3}). For comparison purposes, the mass density is 9.82 g cm^{-3} for Co-9Al-9.8W alloy[7]. However, the γ'-solvus temperature of Co-10Al-5Mo-2Nb alloy decreased to only 866°C and the γ' decomposed after 35h exposure at 800°C[21]. Vanadium is also a promising candidate to replace the high-density W without destabilizing the γ' phase[13,19,23]. However, despite of a high γ'-solvus temperature and a reduced mass density for the Co-Al-V- based superalloys, the high V concentration significantly degrades the hot corrosion resistance, which limits their high-temperature structural applications[24]. All

of these concerns set the stage for the further development and characterization of Co-rich materials for high-temperature applications.

Multicomponent high-entropy alloys are known to display various unique physical and mechanical properties, including high strength both at ambient and elevated temperatures[25–27], and decent irradiation and corrosion resistances[28–30]. Moreover, multicomponent alloys generally offer a feasible approach to resolve the above-mentioned limitations. In this study, we are attempting to fulfill the gap by developing a novel $L1_2$-strengthened multicomponent Co-rich high-entropy alloy with a reduced mass density as well as the superb microstructural stability for advancing the high-temperature mechanical performance. The alloy design strategy is essentially based on the following considerations:(1) Ni additions was used to widen the γ' phase region and suppress the formation of detrimental intermetallic phases[8,23]; (2) alloying additions of Al and Cr to impart in the oxidation resistance as well as to maintain a low γ/γ' lattice misfit[19,31]; (3) using Ti, Mo, Ta, and Nb as substitutions for the high-density W to reduce the mass density while without destabilizing the γ/γ' microstructure[6,14,20]. On the basis of all these considerations, a novel multicomponent Co-rich high-entropy alloy with a composition of $Co_{43.1}Ni_{28.8}Cr_{10.2}Al_{10.0}Ti_{2.1}Mo_{2.2}Ta_{2.1}Nb_{1.5}$ (at.%) was carefully designed and prepared by arc-melting (Table 1), which is referred to as MCoHEA (Multicomponent Co-rich High-Entropy Alloy) hereafter.

An optical microscope was utilized to observe the as-cast dendritic microstructure. Material characterizations were carried out via scanning electron microscope (SEM, Quanta 450), transmission electron microscope (TEM, JEOL 2100F), and atom probe

tomography (APT, CAMECA LEAP 5000 XR). For TEM tests, specimens were first mechanically grounded to a thickness of ~50μm via SiC papers, and then punched into discs with a diameter of 3mm. As followed, thin discs were ion-milled to a level about electron transparency via a precision ion polishing system (Gatan 695). X- ray (a penetration form of the high-energy electromagnetic radi- ation) diffraction (XRD) was utilized for phase identification. The diffraction data were collected from 20° to 100° with a scanning step of 0.02° via a Rigaku high resolution X-ray diffractometer. The electron backscattered diffraction (EBSD) data was acquired from the electropolished specimens using SEM equipped with an Oxford detector. Detailed specimen preparation method was described in our previous studies[27]. The microhardness of the alloy was measured at room temperature as prescribed in American Society for Testing and Materials (ASTM-E92). A Vickers microhardness tester (Fischer HM2000XY) was used to illustrate the temporal microhardness evolutions with a nominal load of 2N and a dwell time of 15s. All microhardness measurements were taken using a set of nine (3 × 3) separate indentations with an average spacing of 300μm. The mass density of the as-cast specimen was determined by a water displacement method at room temperature. Phase transformation temperature was measured by differential scanning calorimeter (DSC, NETZSCH 404C) under an Ar at- mosphere with a constant heating rate of 20°C/min. Tensile tests were conducted at both ambient and elevated temperatures in air with a strain rate of 10^{-2} s^{-1}.

As shown in Fig. 1(a), the as-cast MCoHEA exhibited a dendritic structure with an average second arm spacing of ~10μm. To remove chemical and compositional

inhomogeneity, the as-cast specimen was solutionized at 1200℃ for 2h, followed by coldrolling with a reduction of 50% in thickness and recrystallization at 1200℃ for 2 min. EBSD revealed a homogeneous and fully recrystallized microstructure with randomly distributed grain orien- tations for the as-recrystallized specimen. The average grain size was determined to be 38 ± 5μm (Fig. 1(b)). Subsequently, the samples were subjected to isothermal heat treatments at various temperatures for controlled particle growth. The initial microhardness of the MCoHEA was 310 ± 6HV after cooling from the recrystallization temperature. During isothermal heat treatment at 800℃, it increased dramatically to 407 ± 13 HV after aging for 1h and remained stable thereafter (Fig. 1(c)). To unveil the ori- gin of the strengthening effect, electron microscopy analyses were carried out. Low-magnification SEM image revealed an equiaxed grain structure for the aged sample (Fig. 1(d)). A representative grain boundary region micrograph showed a uniformly distributed high-density γ' particles embedded in the γ matrix (Fig. 1(e)). Noticeably, we did not observe the formation of other intermetallic phases neither at grain boundaries or in the grain interior, which is in good agreement with XRD patterns indicating that only peaks corresponding to the γ-γ' two phases were detected (see Supplementary Fig. S1). Dark-field TEM image also demonstrated the similar morphology, i.e., bright cuboidal-shape γ' pre- cipitates embedded in the dark γ matrix (Fig. 1(f)). The selected area diffraction pattern (SADP) took along [001] zone axis was presented in the inset of Fig. 3(f), which contains the superlattice spots from ordered $L1_2$ precipitates along with fundamental reflec- tions from the γ-(FCC) matrix. Microstructural stability was also carefully examined in the temperature

range from 900℃ to 1100℃, suggesting a stable γ - γ' dual-phase microstructure without detecting other detrimental intermetallic phases (Supplementary Fig. S2). Given the intrinsic metastable nature of the $L1_2$-type γ' phase in Co-based alloy systems, deleterious intermetallic phases were frequently observed among $L1_2$-strengthened Co-based superalloys after long-term thermal exposure, especially at the high-energy grain boundary regions[19,21,32].

The reconstructed nanotip was shown in Fig. 2 via atom probe, showing distinctively different compositions between the disordered FCC matrix phase and the ordered $L1_2$ precipitates (as summarized in Table 1). Partitioning coefficients K_i are calculated to quantitatively illustrate the elemental partitioning behavior (Table 1). Ta and Nb demonstrated a strong tendency to parti- tion to the γ' precipitates, and Ni, Al, Ti, and Mo partially partitioned to the γ' precipitates. In contrast, Co and Cr were depleted in the γ' precipitates and partitioned to the γ matrix ($K_{Cr} = 0.72$ and $K_{Cr} = 0.23$). The findings on the elemental partitioning behavior are in a good agreement with previous work in the field of Co-based alloys[11,15,33]. Omori et al.[34] suggested that ele- ments partitioned to the γ' precipitates ($K_i > 1$) can be considered as the γ' -forming elements, otherwise the γ' -destabilizing elements. Therefore, the Ta and Nb additions in the MCoHEA significantly contribute to the stability of the γ' phase, which agree well with previous findings that 2 at.% Ta and Nb additions increased the γ' -solvus temperature by 82℃ and 57℃ in Co-based alloy, respectively[34]. In contrast, Cr strongly partitioned to the matrix phase, which acts as a γ' -destabilizing element in $L1_2$-strengthened Co-rich alloys and decreases the γ' -solvus temper- ature[35,36].

The γ'-solvus temperature was measured to be 1125℃ for the MCoHEA from DSC heating curves, which is in good agreement with the previous microstructural observations that the sta- ble γ-γ' dual-phase can be retained after aging at 1100℃ (Supple- mentary Fig. S2). For comparison purposes, the γ'-solvus temperatures of other $L1_2$-strengthened Co-based superalloys were plotted in Fig. 3, including (i) Co-Al-W-based superalloys[7,34], (ii) Co-Al-Mo-based superalloys[9,21,22,37], (iii) Co-Ta-V-based super- alloys[19], (iv) Co-Al-V- and Co-Ti-based superalloys[23,31], (iv) Co-Al-Ti-based superalloys[14]. The 1125℃ solvus temperature of the current MCoHEA alloy is substantially higher than those of Co- Al-W-based superalloys (990℃ for Co-9Al-9.8W[7]) and Co-Al-Mo- based superalloys (1021°C for Co-10Ni-7Al-4Ti-5Mo-2Nb[14]). The γ'-solvus temperature in Co-Al-Ti-based superalloys (1134℃ for Co-10Ni-7Al-4Ti-7W-1Ta [14]) is comparable to that of the MCo-HEA. However, a high fraction of heavy element W (7 at.%) is nec- essarily required for the stabilization of γ' particles. More specifically, the mass density of W (19.3 g cm^{-3}) is more than twice the value of Co (8.86 g cm^{-3}) and hence the mass density of Co-10Ni- 7Al-4Ti-7W-1Ta dramatically increased to a value of 9.45 g cm^{-3}[14]. High mass density is unfavorable for engineering applications when the specific strength is crucial, especially for aerospace engineering. In contrast, the mass density of the MCoHEA was mea- sured to be 8.28 g cm^{-3}, which is substantially lower than those of the W-bearing Co-based superalloys, such as Co-9Al-9.8W (9.82 g cm^{-3}) and Co-8.8Al-9.8W-2Ta (9.54 g cm^{-3})[7,34]. Co-Ti-based superalloys preserved a low mass density (8.16 g cm^{-3}) while main- taining a high γ' stability (up to 1100℃ for Co-11Ti-15Cr[31]). The high γ'-

solvus temperature of Co-11Ti-15Cr superalloy is inherent from the thermodynamically stable γ'-Co3 Ti intermetallic compound among Co-Ti binary alloys. However, the high Ti con- tent in Co-Ti-based superalloys deteriorates the oxidation resis- tance at elevated temperatures. Moreover, the Co-Al-V-based superalloys also demonstrated a promising combination of high γ'-solvus temperature and low mass density. However, the elevated V content led to a poor hot corrosion resistance[24]. The carefully controlled γ'-stabilizing elements (Ni, Al, Ti, Nb, Ta, and Mo) contribute to the high γ'-solvus temperature in the MCoHEA. Moreover, it is important to point out that the complete removal of the high-density W element contributes to a reduced mass density in the current MCoHEA. The reduced mass density resulted in an improved specific strength for the current alloy, which is crucial for structural applications.

To examine the temperature dependence of the mechanical properties, tensile tests were conducted for the MCoHEA at both ambient and elevated temperatures.Fig. 4(a) shows the engineering stress-strain curves at 25, 600, 800, and 900°C. The MCo-HEA exhibited decent tensile ductility with the elongation exceeding 20% at ambient temperature. An ultimate tensile strength over 1GPa was achieved in the MCoHEA when tested at 25°C, which can be attributed to the exceptional strain-hardening capabilities at room temperature. The plot between specific yield strength and deformation temperature of the MCoHEA is shown in Fig. 4(b), together with other $L1_2$-strengthened Co-based superalloys[7,9,21,23,31,33,38], solid-solution strengthened Co-based alloys (Haynes 188 and Mar-M-302[39]), and commercial Ni-based superalloy (Waspaloy[40]). It is important to point out that the MCoHEA shows the superior

specific yield strength than that of solid-solution strengthened Co-based alloys over the entire testing temperature range from 25 to 900℃. The specific yield strength of the MCoHEA is also higher than that of most other $L1_2$-strengthened Co-based superalloys. Although the specific yield strength of the MCoHEA is inferior to the commercial Ni-based superalloy Waspaloy at temperatures below 600℃, the MCoHEA outperforms the Waspaloy alloy at temperatures higher than 600℃. Owing to the excellent particle stability, the MCoHEA did not sacrifice much strength even at 900℃, whereas the rapid yield strength degradation can be witnessed at temperatures above 600 °C for the Waspaloy alloy.

Interestingly, we found an anomalous rise in the yield strength of our MCoHEA in the temperature range from 600 to 800℃, and this yield anomaly is attributed to the activation of multiple slip systems at elevated temperatures[41]. Due to the low anti-phase boundary (APB) energies of the {100} plane as compared to those of {111} plane, the screw segments of superdislocations cross slip from {111} plane to {100} plane at elevated temperatures[42,43]. This type of dislocation configuration is also called Kear-Wilsdorf locks, which make the dislocation gliding more difficult and results in the anomalous hardening. Above the peak yielding temperature (800℃), the yield strength slightly dropped to 664 MPa at 900℃. Since we have demonstrated that the γ/γ' dual-phase microstructure is thermodynamically stable in this temperature range and the order-disorder transition temperature is over 1100°C, the possibility of a microstructure degradation is ruled out for the cause of the decreased yield strength above 800℃. The strength loss might be a result of the activation of thermally activated

<112>-type dislocation shearing of the particles above the peak yielding temperature[6,42,44]. Moreover, the shearing of the γ' precipitates is accompanied by the extensive formation of stacking faults, which are reported to be unique for Co-based superalloys when deformed above the peak yielding temperature[44,45]. To make full use of the unusual deformation characteristic found in Co-based alloys, the deformation mechanism in the novel MCoHEA will be examined in further studies for enhancing the high-temperature me- chanical properties.

In summary, a novel multicomponent $L1_2$-strengthened Co-rich high-entropy alloy with a high microstructural stability and superb mechanical performance at elevated temperatures has been developed in the current study. Uniformly distributed high-density cuboidal γ' particles were embedded in the matrix among the MCoHEA subjected to aging treatments at temperatures ranging from 800 to 1100℃. A stable γ / γ' dual-phase microstructure was observed without any brittle intermetallic phase formation neither at grain boundaries nor grain interior after long-term isothermal heat treatments. Distinctly different composition between the γ' - particles and the γ - matrix was revealed by APT. Co and Cr are found to deplete from the γ' particles. Ta and Nb demonstrate a strong tendency to partition to the $L1_2$ precipitates, which act as the γ' -stabilizing elements and contribute to the γ' stability. The MCoHEA also exhibits a synergy between the high γ' -solvus temperature (1125℃) and low mass density (8.28 g cm^{-3}). The present MCoHEA demonstrates superb tensile strength at elevated temperatures, which is higher than that of most $L1_2$-strengthened Co-based superalloys and even superior to that of the Ni-based-superalloy Waspaloy at elevated

temperatures. Our present findings can be exploited for designing advanced $L1_2$ strengthened Co-rich alloys with broader temperature capabilities and the enhanced high-temperature strength. More importantly, the results presented in this study promote the understanding of the precipitation mechanisms and solute partitioning behaviors in $L1_2$-strengthened Co- rich alloys.

Declaration of Competing Interest

The authors declare that they have no known competing financial interests or personal relationships that could have appeared to influence the work reported in this paper.

Acknowledgement

The authors from City University of Hong Kong (CityU) are grateful for the financial support from the Hong Kong Research Grant Council (RGC) with CityU Grant 11213319, 11202718, 9360161, 9610498, as well as the financial support from CityU Shenzhen Research Institute (SRI) (Grant 2020A1515110647). The authors from The Hong Kong Polytechnic University (PolyU) are grateful for the financial support from the Hong Kong RGC (25202719) and internal fund from PolyU (Nos. P0000538, P0009738 and P0013994).

References

[1] J.H. Perepezko, Science 326 (2009) 1068–1069.

[2] 2.B. Cao, T. Yang, W.H. Liu, C.T. Liu, MRS Bull. 44 (2019) 854–859.

[3] T. Yang, Y. Zhao, W. Li, C. Yu, J. Luan, D. Lin, L. Fan, Z. Jiao, W. Liu, X. Liu, C.T. Liu, Science 369 (2020) 427–432.

[4] R. Reed, T. Tao, N. Warnken, Acta Mater. 57 (2009) 5898–5913.

[5] R.C. Reed, The Superalloys: Fundamentals and Applications, Cambridge Univer- sity Press, 2008.

[6] A. Suzuki, H. Inui, T.M. Pollock, Annu. Rev. Mater. Sci. 45 (2015) 345–368.

[7] J. Sato, T. Omori, K. Oikawa, I. Ohnuma, R. Kainuma, K. Ishida, Science 312 (2006) 90–91.

[8] K. Shinagawa, T. Omori, J. Sato, K. Oikawa, I. Ohnuma, R. Kainuma, K. Ishida, Mater. Trans. 49 (2008) 1474–1479.

[9] S. Makineni, A. Samanta, T. Rojhirunsakool, T. Alam, B. Nithin, A. Singh, R. Banerjee, K. Chattopadhyay, Acta Mater. 97 (2015) 29–40.

[10] M. Jin, N. Miao, W. Zhao, J. Zhou, Q. Du, Z. Sun, Comp. Mater. Sci. 148 (2018) 27–37.

[11] F. Xue, H. Zhou, Q. Shi, X. Chen, H. Chang, M. Wang, Q. Feng, Scr. Mater. 97 (2015) 37–40.

[12] [12] B. Cao, C. Wang, T. Yang, C. Liu, Scr. Mater. 187 (2020) 250–255.

[13] F.L.R. Tirado, J.P. Toinin, D.C. Dunand, Acta Mater. 151 (2018) 137–148.

[14] E.A. Lass, D.J. Sauza, D.C. Dunand, D.N. Seidman, Acta Mater. 147 (2018) 284–295.

[15] D.J. Sauza, D.C. Dunand, D.N. Seidman, Acta Mater. 174 (2019) 427–438.

[16] I. Bantounas, B. Gwalani, T. Alam, R. Banerjee, D. Dye, Scr. Mater. 163 (2019) 44–50.

[17] W. Wang, H. Hong, I. Kim, B. Choi, H. Jeong, M. Kim, C. Jo, Mater. Sci. Eng. A 523 (2009) 242–245.

[18] T. Yang, Y. Zhao, L. Fan, J. Wei, J. Luan, W. Liu, C. Wang, Z. Jiao, J. Kai, C.T. Liu, Acta Mater. 189 (2020) 47–59.

[19] F.L.R. Tirado, S. Taylor, D.C. Dunand, Acta Mater. 172 (2019) 44–54.

[20] J. Ruan, W. Xu, T. Yang, J. Yu, S. Yang, J. Luan, T. Omori, C. Wang, R. Kainuma, K. Ishida, Acta Mater. 186 (2020) 425–433.

[21] S. Makineni, B. Nithin, K. Chattopadhyay, Scr. Mater. 98 (2015) 36–39.

[22] S. Makineni, B. Nithin, K. Chattopadhyay, Acta Mater. 85 (2015) 85–94.

[23] Y. Chen, C. Wang, J. Ruan, T. Omori, R. Kainuma, K. Ishida, X. Liu, Acta Mater. 170 (2019) 62–74.

[24] N.S. Patel, V. Pavlík, M. Bocˇa, Crit. Rev. Solid State Mater. Sci. 42 (2017) 83–97.

[25] C. Lee, Y. Chou, G. Kim, M.C. Gao, K. An, J. Brechtl, C. Zhang, W. Chen, J.D.Poplawsky, G.J.A.M. Song, Adv. Mater. 32 (49) (2020) 2004029.

[26] I. Basu, J.T.M. De Hosson, Scr. Mater. 187 (2020) 148–156.

[27] B. Cao, T. Yang, L. Fan, J. Luan, Z. Jiao, C.T. Liu, Mater. Sci. Eng. A 797 (2020) 140020.

[28] Y. Lin, T. Yang, L. Lang, C. Shan, H. Deng, W. Hu, F.J.A.M. Gao, Acta Mater. 196 (2020) 133–143.

[29] J.R. Scully, S.B. Inman, A.Y. Gerard, C.D. Taylor, W. Windl, D.K. Schreiber, P. Lu, Saal, G.S. Frankel, Scr. Mater. 188 (2020) 96–101.

[30] Y. Shi, B. Yang, X. Xie, J. Brechtl, K.A. Dahmen, P.K. Liaw, Corros. Sci. 119 (2017) 33–45.

[31] C.H. Zenk, I. Povstugar, R. Li, F. Rinaldi, S. Neumeier, D. Raabe, M. Göken, Acta Mater. 135 (2017) 244–251.

[32] J.E. Saal, C. Wolverton, Acta Mater. 61 (2013) 2330–2338.

[33] P. Pandey, A.K. Sawant, B. Nithin, Z. Peng, S. Makineni, B. Gault, K. Chattopad- hyay, Acta Mater. 168 (2019) 37–51.

[34] T. Omori, K. Oikawa, J. Sato, I. Ohnuma, U.R. Kattner, R. Kainuma, K. Ishida, Intermetallics 32 (2013) 274–283.

[35] P. Pandey, S.K. Makineni, A. Samanta, A. Sharma, S.M. Das, B. Nithin, C. Srivas- tava, A.K. Singh, D. Raabe, B. Gault, Acta Mater. 163 (2019) 140–153.

[36] D.W. Chung, J.P. Toinin, E.A. Lass, D.N. Seidman, D.C. Dunand, J. Alloys Compd. 832 (2020) 154790.

[37] S. Makineni, B. Nithin, D. Palanisamy, K. Chattopadhyay, J Mater. Sci. 51 (2016) 7843–7860.

[38] Y. Chen, C. Wang, J. Ruan, S. Yang, T. Omori, R. Kainuma, K. Ishida, J. Han, Y. Lu, X. Liu, Acta Mater. 188 (2020) 652–664.

[39] C. Nickel, in: ASM Specialty Handbook, ASM International Materials Park, OH, 2000, p. 44073. -0002.

[40] C.T. Sims, N.S. Stoloff, W.C. Hagel, Superalloys II, Wiley, New York, 1987.

[41] P. Hirsch, Prog. Mater. Sci. 36 (1992) 63–88.

[42] A. Suzuki, T.M. Pollock, Acta Mater. 56 (2008) 1288–1297.

[43] A. Suzuki, G.C. DeNolf, T.M. Pollock, Scr. Mater. 56 (2007) 385–388.

[44] Y. Zhao, T. Yang, Y. Li, L. Fan, B. Han, Z. Jiao, D. Chen, C.T. Liu, J.J. Kai, Acta Mater. 188 (2020) 517–527.

[45] L. Feng, D. Lv, R. Rhein, J. Goiri, M. Titus, A. Van der Ven, T. Pollock, Y. Wang, Acta Mater. 161 (2018) 99–109.

Figure captions

Fig. 1. (a) Optical image of the as-cast MCoHEA, showing dendrite and interdendritic regions. (b) EBSD mapping showing a fully recrystallized microstructure with micronsized equiaxed grains. (c) Temporal microhardness evolution of MCoHEA aging at 800℃. (d) Low-magnifification BSE micrograph of the samples aged at 800℃ for 72h. (e) An enlarged view of the grain boundary triple junction, showing γ /γ dual-phase microstructure. (f) Representative dark-fifield TEM image revealing the high-density cuboidal γ precipitates embed in the γ matrix. Corresponding selected area diffraction pattern (SADP) took along [001] zone axis is shown in the inset. Superlattice spots are highlighted in yellow, suggesting the ordering nature of $L1_2$ particles.

Fig. 2. Atom probe analyses of $L1_2$ particles. (a) Ion maps. 14 at.% Cr iso-concentration surface was used to illustrate the γ / γ' interfaces in the ion map which contains all elements. (b and c) Proximity histograms of individual elements across the γ / γ' interfaces, showing distinctly different elemental compositions between the γ matrix and the γ^J precipitates.

Fig. 3. A comparison of γ' -solvus temperature and mass density of between MCo-HEA and other $L1_2$-strengthened Co-based superalloys.

Fig. 4. (a) Engineering stress-strain curves of the MCoHEA at ambient and elevated temperatures. (b) The plots between specific yield strength and deformation temperature.

Fig 1

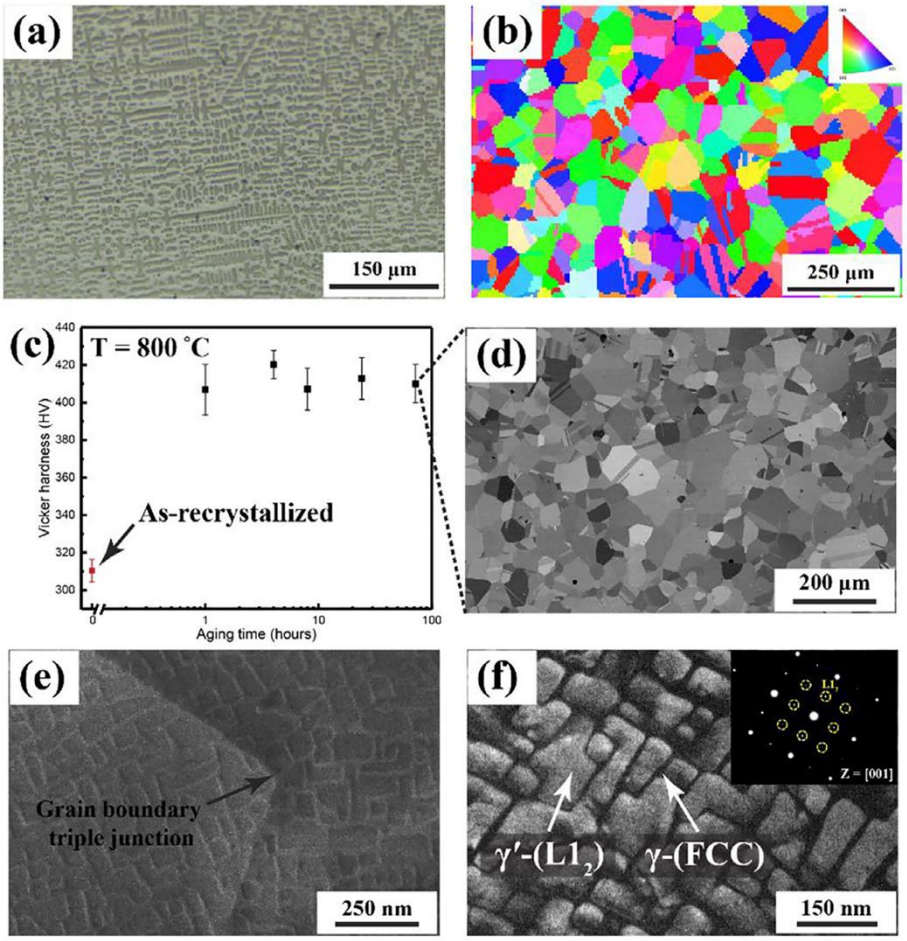
(a)
150 µm
(b)
250 µm
(c)
T = 800 °C
Vicker hardness (HV)
440
420
400
380
360
340
320
300
As-recrystallized
0
1
10
100
Aging time (hours)
(d)
200 µm
(e)
Grain boundary
triple junction
250 nm
(f)
Z = [001]
γ′-(L1$_2$)
γ-(FCC)
150 nm

Fig 2

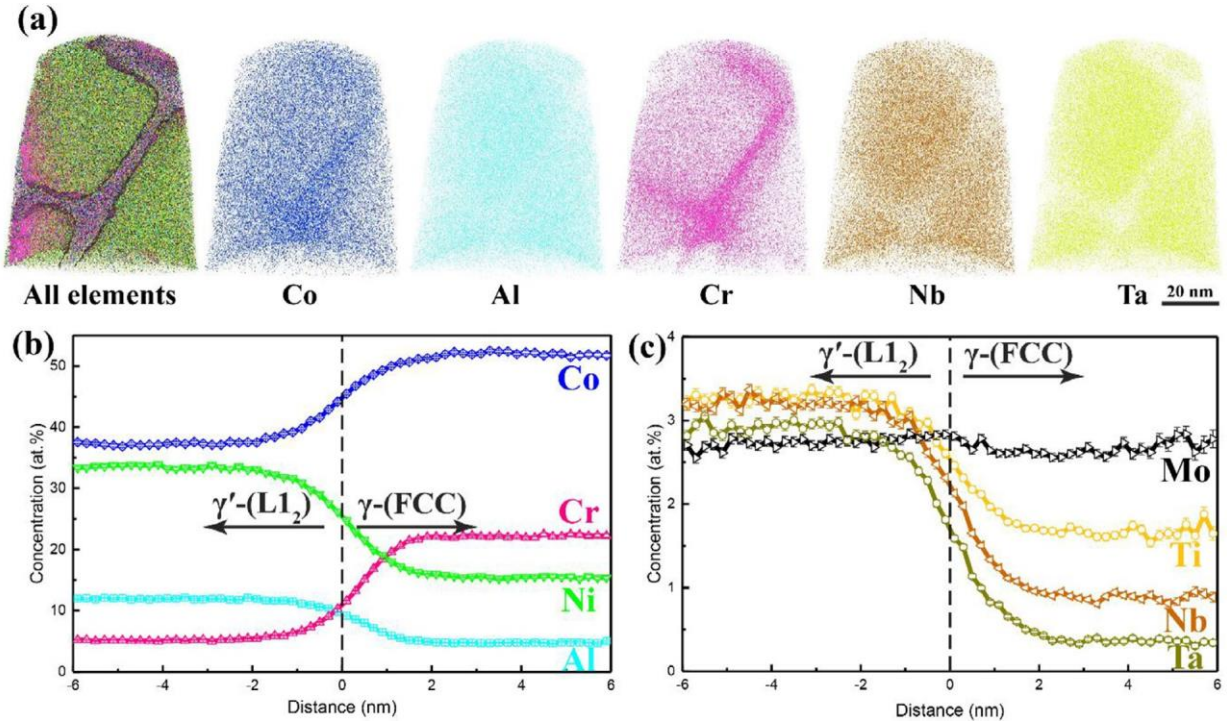
(a)
All elements
Co
Al
Cr
Nb
Ta
20 nm
(b)
Co
Cr
Ni
Al
γ′-(L1$_2$)
γ-(FCC)
Concentration (at.%)
Distance (nm)
(c)
γ′-(L1$_2$)
γ-(FCC)
Mo
Ti
Nb
Ta
Concentration (at.%)
Distance (nm)

Fig 3

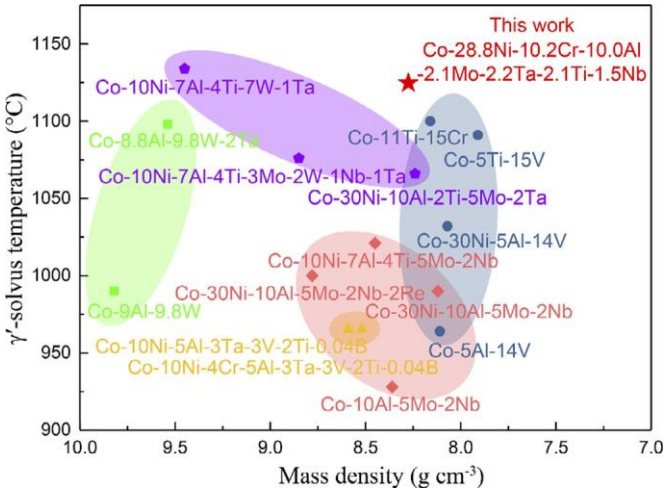
This work
Co-28.8Ni-10.2Cr-10.0Al
-2.1Mo-2.2Ta-2.1Ti-1.5Nb
Co-10Ni-7Al-4Ti-7W-1Ta
Co-8.8Al-9.8W-2Ta
Co-11Ti-15Cr
Co-5Ti-15V
Co-10Ni-7Al-4Ti-3Mo-2W-1Nb-1Ta
Co-30Ni-10Al-2Ti-5Mo-2Ta
Co-30Ni-5Al-14V
Co-10Ni-7Al-4Ti-5Mo-2Nb
Co-30Ni-10Al-5Mo-2Nb-2Re
Co-9Al-9.8W
Co-30Ni-10Al-5Mo-2Nb
Co-10Ni-5Al-3Ta-3V-2Ti-0.04B
Co-5Al-14V
Co-10Ni-4Cr-5Al-3Ta-3V-2Ti-0.04B
Co-10Al-5Mo-2Nb
γ′-solvus temperature (°C)
Mass density (g cm-3)
1150
1100
1050
1000
950
900
10.0
9.5
9.0
8.5
8.0
7.5
7.0

Fig 4

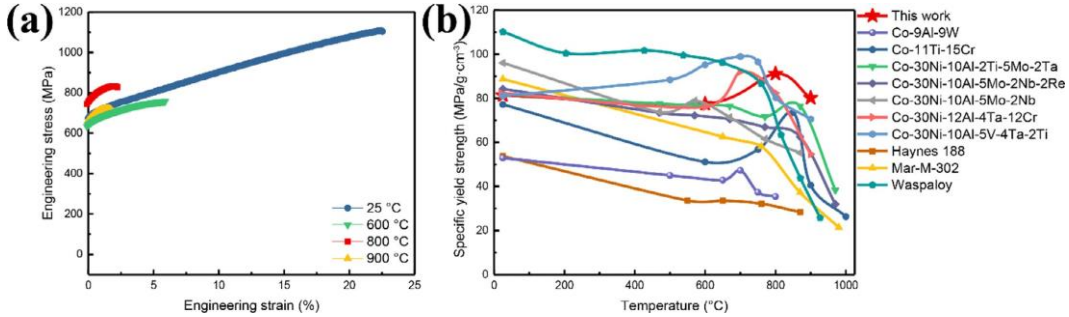
(a)
Engineering stress (MPa)
Engineering strain (%)
25 °C
600 °C
800 °C
900 °C
(b)
Specific yield strength (MPa/g·cm⁻³)
Temperature (°C)
This work
Co-9Al-9W
Co-11Ti-15Cr
Co-30Ni-10Al-2Ti-5Mo-2Ta
Co-30Ni-10Al-5Mo-2Nb-2Re
Co-30Ni-10Al-5Mo-2Nb
Co-30Ni-12Al-4Ta-12Cr
Co-30Ni-10Al-5V-4Ta-2Ti
Haynes 188
Mar-M-302
Waspaloy